JOURNAL OF SOLID STATE CHEMISTRY 120, 332–342 (1995)

Structural Aspects of Modulated Superconducting Oxides: Application to $Hg_{1-x}Tl_xSr_{4-y}Ba_yCu_2CO_3O_{7-\delta}$

M. Huvé,* G. Van Tendeloo,*,[1] S. Amelinckx,* M. Hervieu,† and B. Raveau†

* *EMAT, University of Antwerp (RUCA), Groenenborgerlaan, 171, B-2020 Antwerpen, Belgium; and † CRISMAT, ISMRA, Université de Caen, Boulevard Maréchal Juin, F-14050, Caen Cedex, France*

Received April 24, 1995; accepted August 3, 1995

Superconducting oxides of the type $Hg_{1-x}Tl_xSr_{4-y}Ba_yCu_2CO_3O_{7-\delta}$ show complex modulated structures with a modulation vector along [010] and a wavelength varying between 6 and 8 times the basic perovskite unit. High resolution electron microscopy indicates that the modulation is introduced by an ordering of CO_3 groups on the (Hg–Tl) sublattice. Such modulated structures are discussed in general; they are the result of a minimization of the internal stresses due to the differences in ionic sizes of the constituents. © 1995 Academic Press, Inc.

INTRODUCTION

A wide variety of novel superconducting materials has recently been prepared by incorporating complex ions such as carbonate, phosphate, or sulfate groups in the perovskite like structures of existing high Tc cuprates. In this paper we shall particularly focus our attention on the substitution of carbonate groups in the mercury and thallium based cuprates of the type $Hg_{1-x}Tl_xSr_{4-y}Ba_yCu_2CO_3O_{7-\delta}$(I) where the incorporation of carbonates produces interesting modulated structures. Related compounds of the type $ASr_{4-y}Ba_yCu_2CO_3O_{7-\delta}$(II) where A = Tl, Hg and $y = 2$ or $A = Hg_{0.5}Pb_{0.5}$; $y \neq 2$ have been studied previously (1–5). They were found to exhibit remarkable long period interface modulated structures. The modulation vector is along the $[010]_p$ direction in the samples with A = Tl, whereas it is along the $[110]_p$ direction in the samples with A = Hg or $A = Hg_{0.5}Pb_{0.5}$.

The objective of the research reported here was to study the effect of variations of the Sr/Ba ratio and of the Hg/Tl ratio in compounds of the type (1) on the structure or microstructure and on their superconducting properties. We shall describe the microstructure as determined by electron diffraction and electron microscopy and we shall further show that it is to a large extent determined by a strain energy minimization principle. The same principle will be shown to apply, at least in part, to a number of other modulated structures of superconductors.

EXPERIMENTAL DETAILS

The compounds were synthesized by the solid state reaction of a mixture of Tl_2O_3, HgO, $SrCO_3$, $BaCuO_2$, $SrCuO_2$, and CuO in the appropriate proportions to realize a normal oxygen content of O_{10}. The fine powders were mixed in an agate mortar, pressed into pellets, which were heated for 14 hr at 850°C in an alumina cruicible sealed in an evacuated quartz ampoule, and subsequently quenched to room temperature.

X-ray diffraction patterns were obtained with a Philips XRD diffractometer for the $K\alpha$ radiation in the range $6° \leq 2\theta \leq 100°$. Energy dispersive microanalysis was performed with a Kevex spectrometer. High resolution images and electron diffraction were obtained in a Jeol 4000EX and a Philips CM20 microscope. Superconducting properties were measured by means of a squid magnetometer in zero-field-cooled mode with an applied field of 5 G. No demagnetization corrections were made.

RESULTS FOR $Hg_{1-x}Tl_xSr_{4-y}Ba_yCu_2CO_3O_{7-\delta}$.

Quasi-single-phase material with formula (I) was obtained for the following values of the parameters x and y:

$$0 < x < 1 \quad \text{for } y = 2$$

$$2 < y < 3 \quad \text{for } x = 0.5.$$

Samples with nominal compositions corresponding to $x = 0$; $y = 2$ and $x = 1$; $y = 2$ were studied earlier (1–4). In this paper we discuss in particular the observations in samples with compositions $x = 0.7$; $y = 2$ and $x = 0.7$; $y = 3$. Using EDX microanalysis to measure the Hg, Tl, Ba, and Sr content, it was found that the crystals of a given sample all had the same concentration ratio, showing the homogeneity of the samples. Nominal and measured composi-

[1] To whom correspondence should be addressed.

0022-4596/95 $12.00

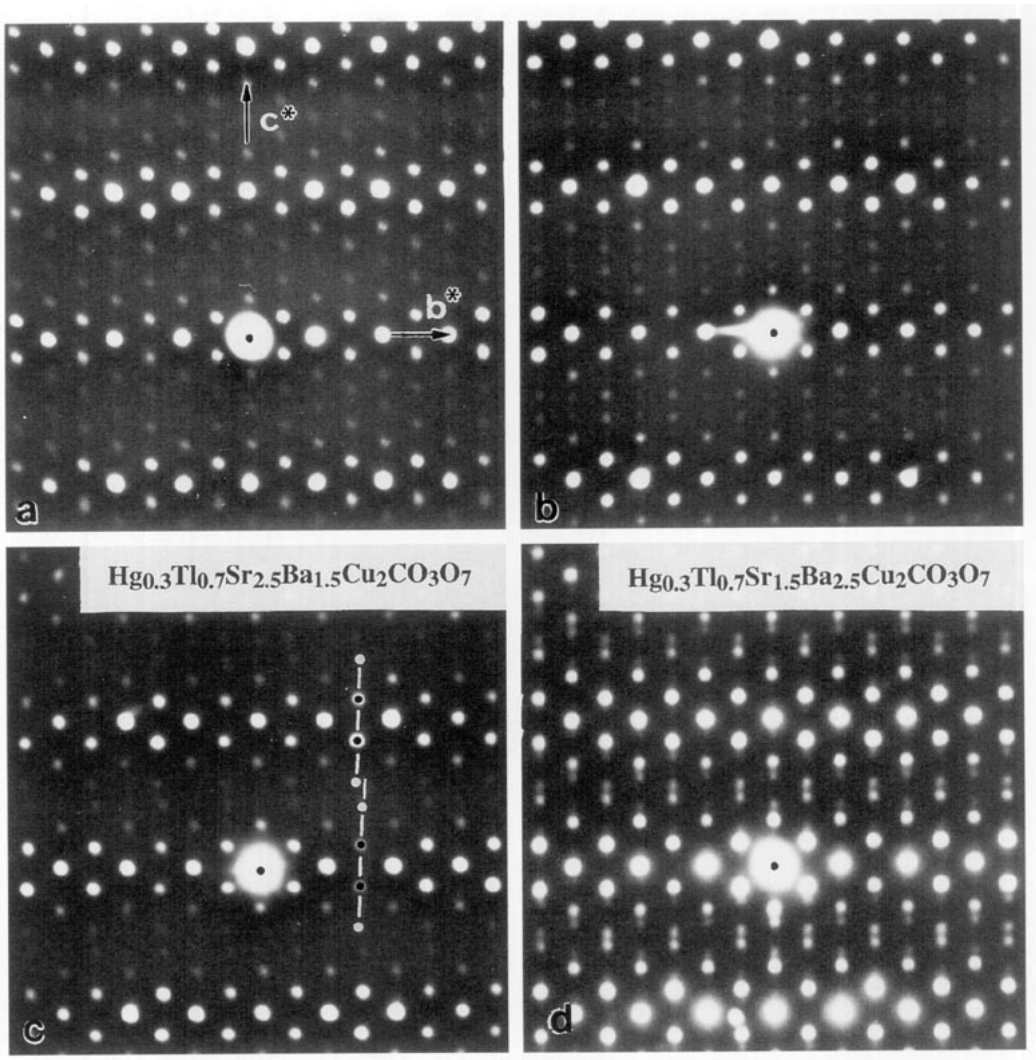

FIG. 1. [100] electron diffraction patterns of: (a) $Hg_{0.3}Tl_{0.7}Sr_{2.5}Ba_{1.5}Cu_2CO_3O_{7-\delta}$; the pattern is quasi-commensurate with $\lambda = 7.66d_{010}$. (b) $Hg_{0.3}Tl_{0.7}Sr_{2.5}$ $Ba_{1.5}Cu_2CO_3O_{7-\delta}$; the pattern is slightly incommensurate with $\lambda = 7.04d_{010}$. (c) $Hg_{0.3}Tl_{0.7}Sr_{2.5}Ba_{1.5}Cu_2CO_3O_{7-\delta}$; the pattern is incommensurate with $\lambda = 7.04d_{010}$, a spacing anomaly is clearly present. (d) $Hg_{0.3}Tl_{0.7}Sr_{1.5}Ba_{2.5}Cu_2CO_3O_{7-\delta}$; the pattern is strongly incommensurate with $\lambda = 6.47d_{010}$.

tions usually differ; in particular the nominal Ba content is systematically smaller than that actually measured. This is presumably due to the presence of unreacted $BaCO_3$. The specimens are clearly mixed crystals of mercury and thallium and of barium and strontium. The lattice parameters, as deduced from the X-ray diffraction patterns (6), show that a and c increase with y; i.e., on substituting Ba for Sr.

$$Hg_{0.3}Tl_{0.7}Sr_{1.5}Ba_{2.5}Cu_2CO_3O_7 \rightarrow a = 3.908(1)\ \text{Å};$$
$$b = 25.325(4)\ \text{Å};\ c = 16.850(2)\ \text{Å}$$
$$Hg_{0.3}Tl_{0.7}Sr_{2.5}Ba_{1.5}Cu_2CO_3O_7 \rightarrow a = 3.898(1)\ \text{Å};$$
$$b = 29.661(5)\ \text{Å};\ c = 16.685(2)\ \text{Å}$$

This can be understood by noting that the Ba^{2+} ion is larger than the Sr^{2+} ion for the same coordination. The differences in the b parameter, i.e., of the modulation wavelength, will be discussed below.

The as synthesized Hg–Tl oxycarbonates are superconducting with Tc close to 65 K ($y = 2.5$) and 60 K ($y = 1.5$). The diamagnetic volume fractions, close to 70 and 40%, respectively, confirm the bulk character of the superconductivity. After annealing under a reducing H_2/Ar flow at 300°C, the critical temperatures slightly increase to 67 and 65 K. On the other hand, annealing under oxygen flow makes Tc decrease, but with an unaltered diamagnetic volume fraction. These results strongly indicate that the slightly overdoped samples are close to being optimized in the as synthesized condition.

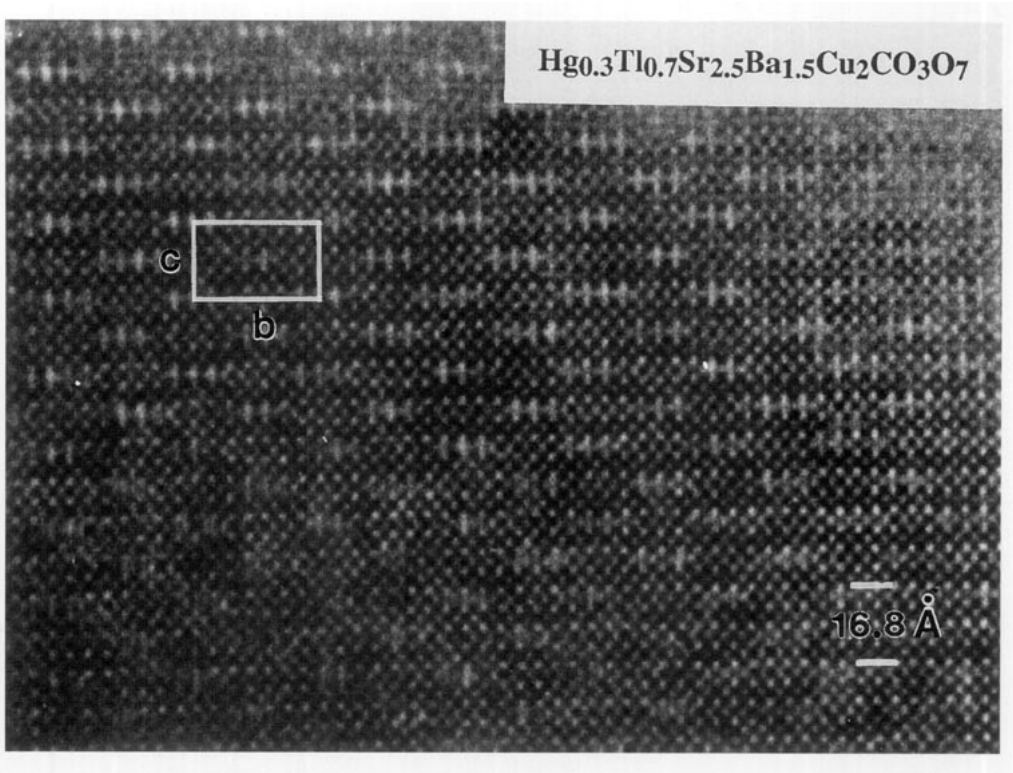

FIG. 2. HREM image of $Hg_{0.3}Tl_{0.7}Sr_{2.5}Ba_{1.5}Cu_2CO_3O_{7-\delta}$ along [100].

Electron Diffraction Evidence of $Hg_{0.3}Tl_{0.7}Sr_{2.5}Ba_{1.5}Cu_2CO_3O_{7-\delta}$

The most relevant zone of reciprocal space is the [100], since it reveals the modulation. The [100] zone pattern for the compound $x = 0.7$; $y = 1.5$ is represented in Figs. 1a–1c. It consists of main reflections which can be indexed on a tetragonal lattice with $a_P = 3.8$ Å and $c_P = 16.5$ Å in agreement with the X-ray results and of somewhat weaker satellite reflections, which decrease in intensity with distance from the main reflections. The pattern looks commensurate, however careful measurements show that it is in fact slightly incommensurate, the period being slightly smaller than $8b_p$. The diffraction conditions suggest a space group *Ammm* or *Amm*2.

A number of specimens of the same sample produce a pattern such as Fig. 1b, which superficially again looks commensurate. However, the rows of the satellite reflections parallel to c^* are slightly zigzag shaped, revealing again a small incommensurability, the wavelength of the modulation being slightly smaller than $7b_p$. In a small number of crystals from the same sample, diffraction patterns such as in Fig. 1c were observed. It is clear that the sequences of satellites are not exactly parallel to the basic lattice row; there is a so-called "orientation anomaly" next to a "spacing anomaly." The wavelength of the modulation is the same as in the pattern of Fig. 2b, i.e., slightly smaller than $7b_p$.

Electron Diffraction Evidence of $Hg_{0.3}Tl_{0.7}Sr_{1.5}Ba_{2.5}Cu_2CO_3O_{7-\delta}$

In specimens of this sample the [100] zone diffraction pattern looks typical as shown in Fig. 1d; a spacing anomaly is obvious. The modulation wavelength is somewhat larger than 6. Although it is clear that the variability of the modulation wavelength within the same sample precludes a simple relation between composition and modulation wavelength, we can nevertheless conclude that the wavelength tends to decrease as the ratio Ba/Sr increases at a constant Hg/Tl ratio.

High Resolution Imaging of $Hg_{0.3}Tl_{0.7}Sr_{4-y}Ba_yCu_2CO_3O_{7-\delta}$

High resolution images corresponding to the diffraction patterns of Figs. 1a and 1d were obtained; they are reproduced in Figs. 2 and 3. Similar images have been interpreted previously, supported by image simulations (5, 6). It was shown in particular that the prominently bright dot sequences image columns of carbon and oxygen atoms which are the lightest atoms in the compound. A similar interpretation applies to the present case. The gaps between the sequences of prominently bright dots are occupied by short sequences of prominently dark dots which can be interpreted as the images of mixed columns of mercury and thallium, the heaviest atoms in the compound. The remaining

dot rows are consistent with the [100] zone view of the perovskite blocks. The sequences contain either three or four dots. Bright and dark dot sequences alternate in antiphase in successive layers, leading to a centered rectangular arrangement of sequences of each kind. Observing the photograph at grazing incidence along a direction perpendicular to the layers it becomes obvious that quasi-periodically darker stripes are present; they are easily visible in an inclined photograph of this image (Fig. 2b). These stripes can be attributed to the presence of dots with an intermediate brightness, presumably due to a mixed composition of the columns limiting the dot sequences.

The separation of the dark dots is significantly smaller than that of the bright dots within the same layer, as shown in Fig. 3b. The separation in the dot rows corresponding with the CuO_2 layer, i.e., midway between the layers containing the short sequences, is intermediate between that of the dark and that of the bright dots as indicated in Fig. 3b. Note that the layers in the perovskite blocks are wavy; their minimum separation along c coincides with the positions of the CO sequences, the maximum with that of the Tl–Hg sequences.

The waviness of the layer planes is coupled to waviness of the planes vertical to these layers because the latter tend to remain locally perpendicular to the wavy layers. These two orthogonal sets of waves are represented schematically in Fig. 4. Where the interlayer spacing within the mixed layers is largest (i.e., in the CO sequences), the interlayer spacing of the adjacent (Sr–Ba)O layers is smallest and vice versa. This suggests that the ion size within the mixed layer is not the main cause determining the interlayer spacing. The elastic model to be discussed below is consistent with these observations.

MODELS FOR THE $Hg_{1-x}Tl_xSr_{4-y}Ba_yCu_2CO_3O_{7-\delta}$ SUPERSTRUCTURE

The high resolution images suggest a model for the modulated structure of these compounds. The succession of layers along the c direction is

$$[CO + (Tl, Hg)O_\delta]\text{–}(Sr, Ba)O\text{–}CuO_2\text{–}$$
$$(Sr, Ba)O\text{–}[(Tl, Hg)O_\delta + CO].$$

The compound is in fact a derivative of the prototype "1201" structure:

$$HgO_\delta\text{–}BaO\text{–}CuO_2\text{–}BaO\text{–}HgO_\delta.$$

In the present compound, the HgO layers contain quasi equally wide strips of (Hg, Tl)O and of CO, parallel to the [100] direction. The period along [010] of the modulated structure is determined by the average width of these strips. Incommensurate diffraction patterns are produced by structures in which commensurate strips of two different widths (3 and 4 times a_P) are uniformly mixed. The high resolution images, as well as the $\mathbf{q}$ vectors deduced from the satellite sequences, give evidence for sequences such as 3434 ... or 334334 ... (Figs. 2 and 3). The fourth dot in a sequence can often be assigned equally well to either the left or the right sequence since it consists of a mixed column (Hg–Tl)O.

Considering the superstructure with homogeneous layers,

$$(Tl, Hg)O\text{–}(Sr, Ba)O\text{–}CuO_2\text{–}(Sr, Ba)O\text{–}CO\text{–}$$
$$(Sr, Ba)O\text{–}CuO_2\text{–}(Sr, Ba)O\text{–}(Tl, Hg)O,$$

as the basic structure, the modulated structure can be described as a long period antiphase boundary structure derived from this structure by a shear with a displacement vector along the c direction equal to $1/2\ c_{sup}$ and with interfaces in the (010) planes. In such a structure all layers, except the (Hg–Tl)O and the CO layers, remain continuous, but the strips of (Hg–Tl)O or CO columns now adopt a centered rectangular arrangement causing A-centering of the modulated structure unit cell and leading to the diffraction conditions for $h0l$ reflections: $h + l$ = even, as observed.

In certain crystallites these antiphase boundaries are not strictly perpendicular to the family of antiphase boundary planes; they enclose a small angle with the [010]* direction, as in Fig. 1c. Similar orientation anomalies were first observed in periodic antiphase boundary structures in the $Au_{4-x}Zn$ system (7).

GENERAL DISCUSSION ON MODULATED STRUCTURES

The structures under discussion are schematized in Fig. 5. Alternating P layers are infinitely extended. They are sandwiched by layers which consist of parallel strips of constant width, alternating strips having different structures, A and B, creating hereby a long period superstructure with a long lattice parameter equal to twice the strip width. Along the superlattice direction the interplanar spacing of the planes normal to this direction is called d_P. The corresponding interplanar (or interrow) spacings of the A and B structures, when occurring in separate crystalline phases, are called, respectively, d_A and d_B. The three spacings d_P, d_A, and d_B defined in this manner are in general different but the P lamellae and the A and B layers may nevertheless form a mixed layer structure with a stacking sequence $APBPAPBP$, provided the differences between d_P, d_A, and d_B are small enough. If we assume that such a structure exists, it is clear that then $d'_A \approx d'_B \approx d'_P \approx d_0$

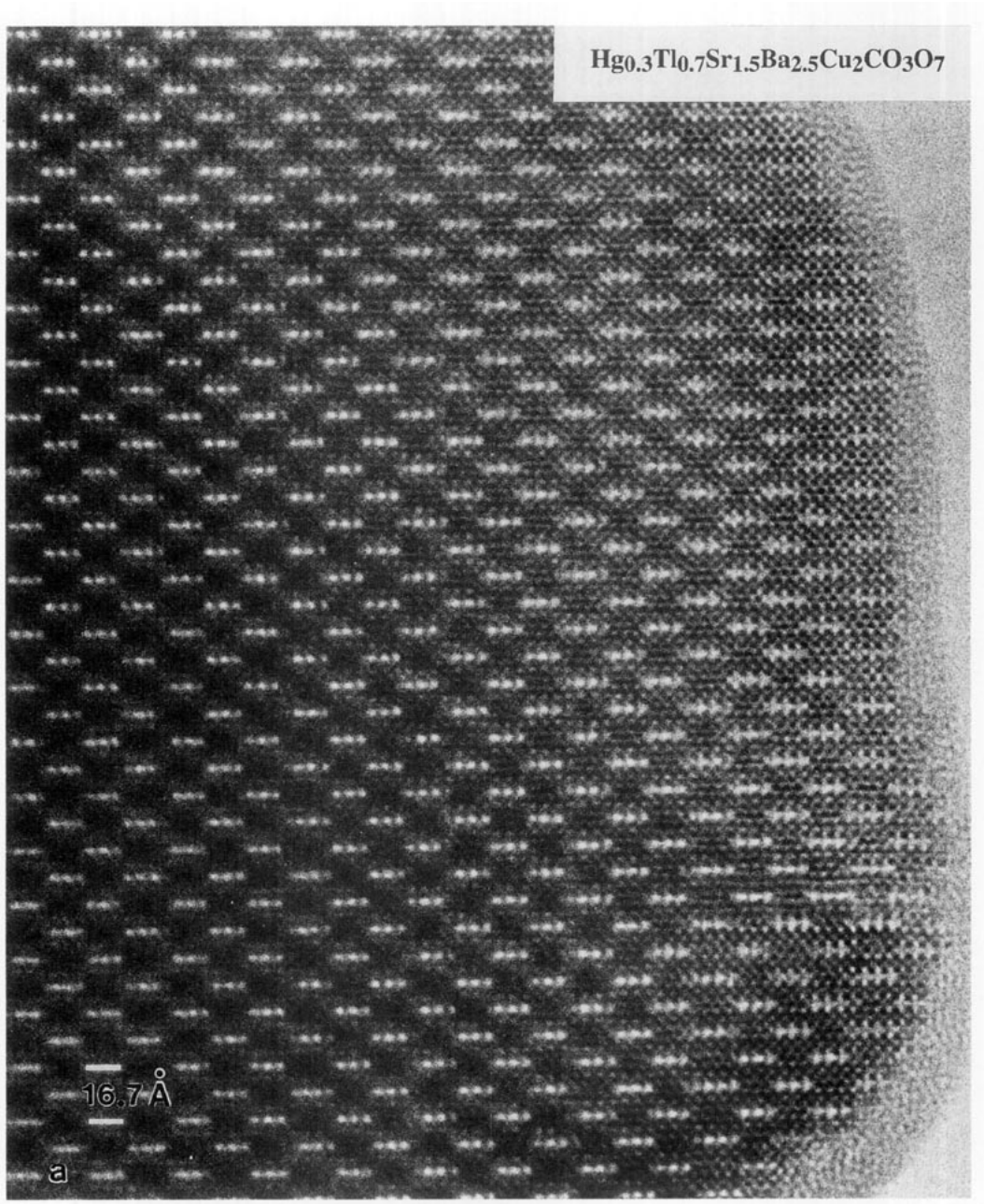

FIG. 3. (a) HREM image of $Hg_{0.3}Tl_{0.7}Sr_{1.5}Ba_{2.5}Cu_2CO_3O_{7-\delta}$ along [100]. (b) Image photographed under grazing incidence. (c) Higher magnification indicating the differences in spacing.

is the average interplanar (interrow) spacing of this layer structure after relaxation (the dashes refer to spacings after relaxation); this is the spacing as determined by a diffraction experiment. Since in general d_A, d_B, and d_P are different from d_0 the layers will be strained in a direction parallel to the layers and one will still have small residual differences between d'_A, d'_B, and d'_P.

For layers of tetragonal symmetry, as is the case in all considered structures, the misfit is two-dimensional. However, it is found empirically that usually relaxation along one direction predominates in any given area, giving rise to a small orthorhombicity of the basic structure and to a long period modulated structure in only one out of two possible directions. In the bismuth cuprates this gives rise to 90° rotation twins of the modulated structure (8). Purely geometrical considerations based on a hard sphere model, which is not too bad for ions, allow one to understand this. Consider the layer of Fig. 6 representing for instance a (001) Tl–O layer with sodium-chloride-like configuration. In this structure the atoms touch along the ⟨110⟩ directions.

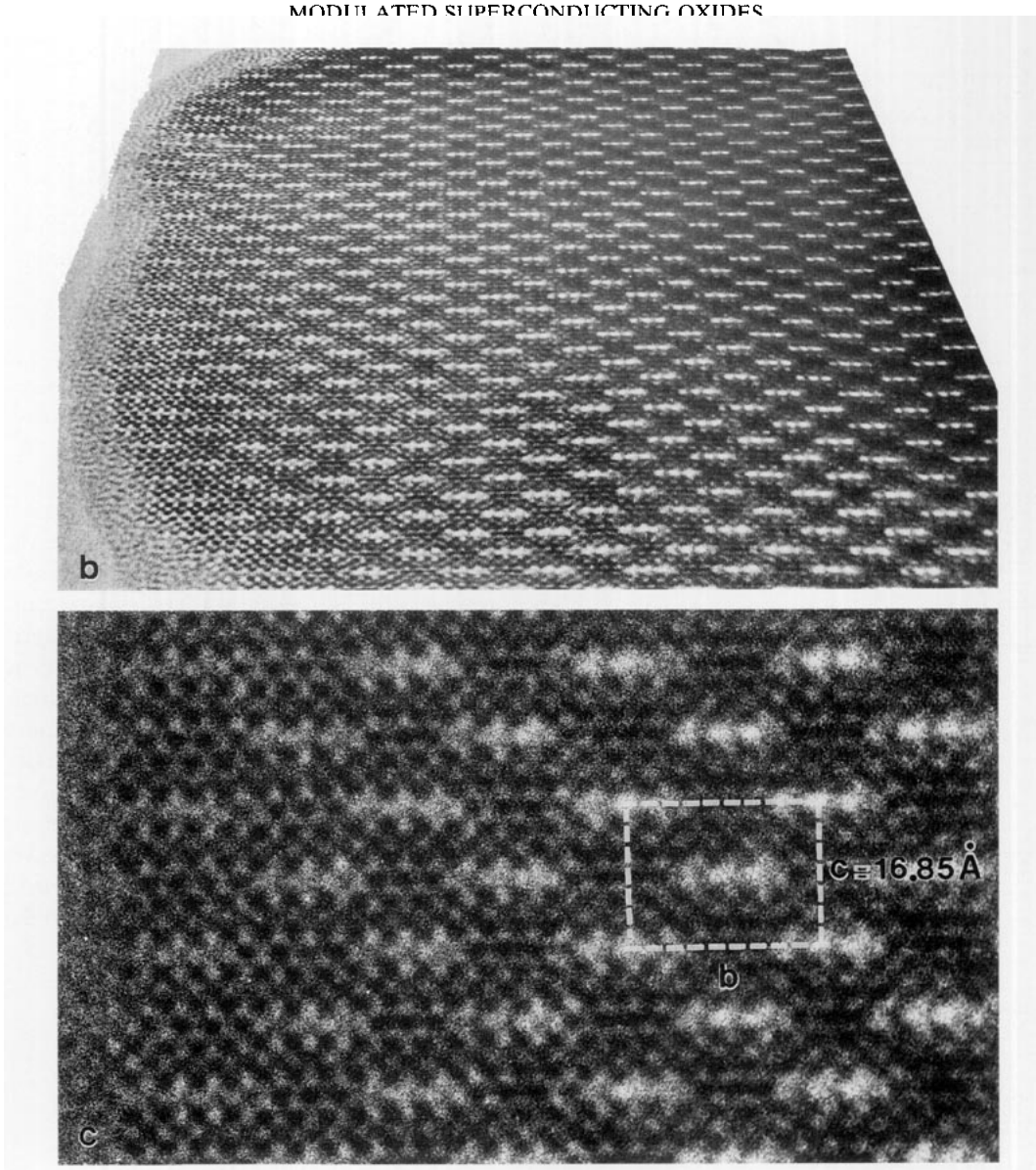

FIG. 3—*Continued*

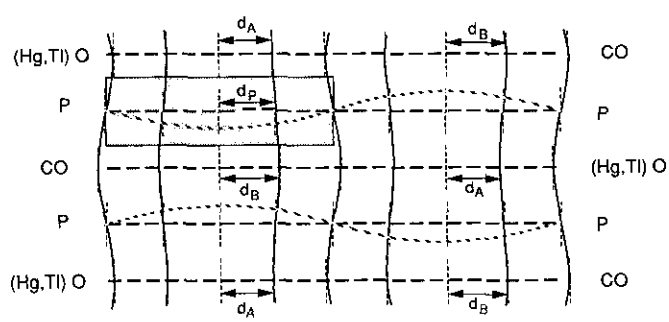

FIG. 4. Realistic model of the resulting configuration where the strain energy is minimized.

If the atoms (1) and (4) as well as (2) and (3) tend to relax toward one another in order to fit the substrate *P* layer, the separation of the pairs (1) and (2) as well as (3) and (4) increases and the unit mesh becomes rectangular. If good fit is achieved through relaxation in one direction the fit will necessarily be worse in the perpendicular direction, which will become the direction of long period modulation. This relaxation is a cooperative phenomena and adjacent unit meshes will tend to relax in parallel directions; hence domains of the different modulation variants may occur in the cuprates (8).

The value of d_0 defined above will be intermediate between the largest and smallest of the three spacings. In the particular case of interest here the *P* layer (perovskite) is

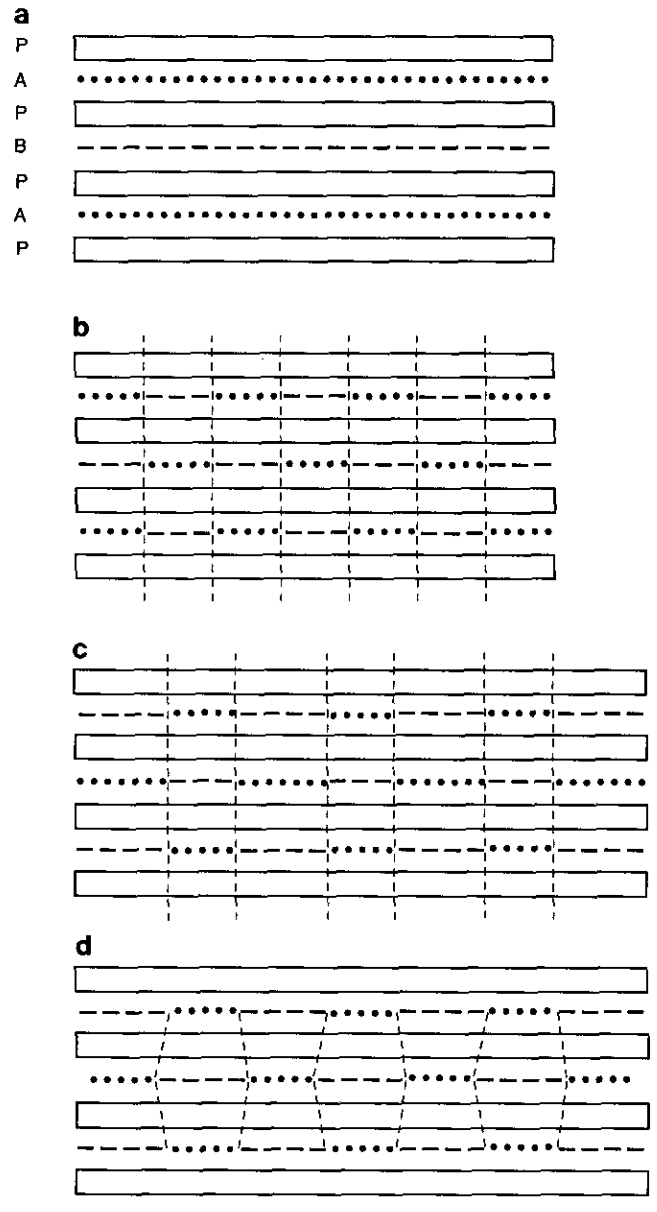

FIG. 5. Schematic structural models for perovskite based structures consisting of perovskite blocks (P), sandwiched between two different layers containing A (e.g., Hg) and B (e.g., CO) atoms.

assumed to be the most incompressible one and therefore it largely determines the lattice spacing $d_P \approx d_0$. Four different situations can logically be envisaged.

$$\text{(i)}\ d_A < d_P < d_B$$

$$\text{(ii)}\ d_A > d_P > d_B$$

$$\text{(iii)}\ d_A > d_P < d_B$$

$$\text{(iv)}\ d_A < d_P > d_B$$

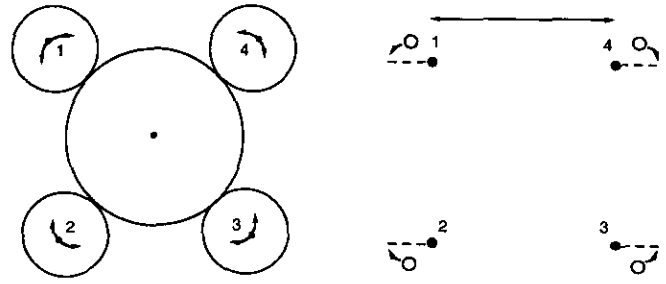

FIG. 6. Hard sphere model of the NaCl type layer, where the ions touch along the ⟨110⟩ directions. The original configuration (left) relaxes into (right) in order to adapt to a larger or smaller perovskite block.

Situations (i) and (ii) (see also Fig. 7) are not essentially different. In the $APBPAPB\ldots$ structure the A layers are now under tensile stress and the B layers are under compressive stress for situation (i). For situation (ii), A and B are interchanged. The situations (iii) and (iv) are also closely related. In (iii), the A and B layers are under compressive stress and the P lamellae are under tensile stress. In (iv), all stresses are reversed as compared to those in (iii). If the differences in interplanar spacings are smaller than a certain limit, (iii) and (iv) will give rise to stable structures with infinite layers, atoms occupying relaxed positions, possibly breaking the fourfold symmetry, as described above. Creating layers consisting of an alternation of A and B strips does not allow one to avoid a cummulative

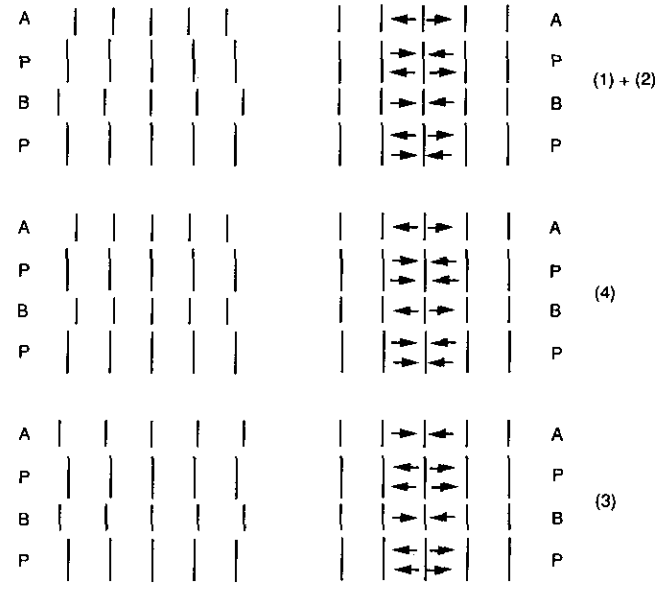

FIG. 7. Schematic representation of four different situations according to the relative magnitude of the interplanar distances d_A, d_B, and d_P (left), together with the resulting stress patterns (right). (top) $d_A < d_P < d_B$ or $d_A > d_P > d_B$; (middle) $d_A > d_P < d_B$; (bottom) $d_A < d_P > d_B$.

misfit and hence does not eliminate long range stresses; misfit dislocations could be introduced if the misfit exceeds a certain limit, which depends on the nature of the layers and in particular on their elastic properties. This is assumed not to happen in the cases under consideration here.

The situation is quite different in the cases (i) and (ii). Creating mixed A–B layers, consisting of an alternation of parallel A and B strips, now allows one to relieve the long range stresses. This is shown schematically in Figs. 5b–5d. Provided the composition is such that the layers A and B can cover the same total surface area, the strain will be minimized if the strips of A and B are equally wide. It looks as if in the limit it would be sufficient to create a mixed layer consisting of an alternation of single rows of A and B structure to achieve an optimum relief of the stresses; a short period superstructure would then result in these layers. This, however, does not necessarily correspond to the configuration of lowest energy. From the assumption that the structure $APBPAPBP\ldots$ is stable, at least for P lamellae with a suitable interplanar spacing, we conclude that creating a borderline between a strip of A and a strip of B structure costs energy comparable to an antiphase boundary energy; i.e., within the (A, B) layers there is no tendency for ordering but rather more for clustering. The energy cost associated with the boundary lines between A and B strips has to be balanced against the energy gain due to the reduction of the misfit strains. The energy due to the residual misfit strain clearly increases with the width of the strips since the misfit is cummulative. The strain energy scales with the square of the strain, i.e., roughly with the square of the strip width. The energy associated with the boundary lines between strips increases with the density of such lines and is thus proportional to the inverse of the width. These two contributions are shown schematically in Fig. 8. It is clear that an optimum strip width, corresponding to the energy minimum, will occur. Qualitatively speaking the strip width will decrease as the misfit increases and vice versa, assuming the boundary line energy to remain the same. For constant values of d_A and d_B the optimum strip width will still depend on d_P. It is possible that the optimum width is equal to a noninteger number of interplanar spacings. In this case uniform sequences of strips with two different widths, differing by one interplanar spacing, occur. In such cases the superstructure diffraction pattern may look incommensurate. The boundary line between A and B strips need not be sharp. Rows consisting of a mixture of atoms belonging to the A and B structures may cause a gradual transition along the boundary line between the two strips.

The second feature, which follows also from the same principle, is the fact that the modulation waves are arranged in such a way that a centered rectangular unit mesh results. This configuration is again to be expected on the basis of the strain energy minimization principle. Along a given A–B layer strips of compressive stress alternate with strips of tensile stress. On stacking such layers the interaction strain energy will be minimized if regions of tensile stress overlap, to the largest extent possible, regions of compressive stress. Such a situation is realized in the model of Fig. 4 where also along the direction perpendicular to the layer planes regions of compressive and tensile stress alternate. The resulting strain causes a slightly sinusoidal shape of the lattice planes in the P lamellae, the curvature being out of phase in adjacent layers.

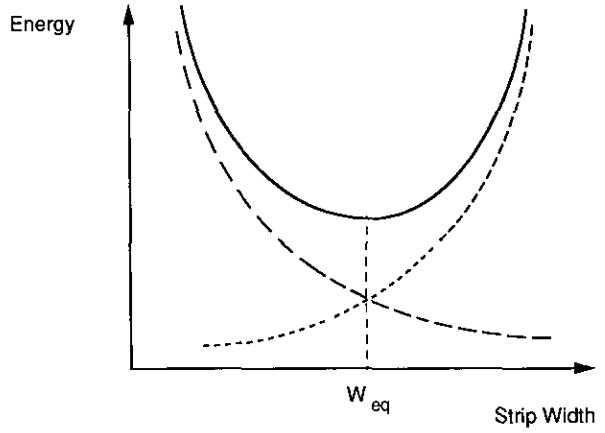

FIG. 8. Schematic plot of the free energy versus the strip width (full line). The energy associated with the boundary lines (dashed line) is decreasing with increasing width; the energy due to the misfit (dotted line) increases with the width.

The fractional misfit between two square lattices with slightly different lattice parameters is of course the same along all crystallographic directions within (001), at least before relaxation. However the elastic properties of a cubic crystal are in general anisotopic, even in a plane perpendicular to a fourfold axis. The strain energy associated with the misfit, i.e., with the atom relaxations, will then be different for different $[hk0]$ directions in the (001) plane, not related by symmetry; it will moreover depend on the chemical composition and on the associated structure. It is possible that in one compound the d_{110} interplanar spacing is more adaptable than d_{100} or vice versa. This is expressed in the term describing the misfit strain energy by a different proportionality factor, which depends on the elastic constants. Also, the energy cost associated with a boundary line depends in general on its orientation within the (001) plane. In particular the presence of oxygen vacancies in the rocksalt-type layers with composition $(Hg, Pb)O_{1-\delta}$ and $(Hg, Tl)O_{1-\delta}$ may significantly influence the anisotropy of the elastic properties in such a way that relaxation along $[110]p$ is preferred over $[100]p$, especially if the distribution of the vacancies would not be isotropic.

As mentioned above, the strip widths nd_A and md_B are limited by the maximum strain ε_{max} which can be accomo-

dated elastically, which means in such a way that the numbers of unit meshes remain equal in all superposed layers. This imposes the conditions

$$n(d_p - d_A) \leq \varepsilon_{max} \quad [1]$$

$$m(d_B - d_p) \leq \varepsilon_{max}. \quad [2]$$

m and n are integral numbers of unit cells of type A and/or type B in one of the mixed layers in Fig. 5.

It is clear that the larger $d_p - d_A$ or $d_B - d_p$, the smaller m and n will be, i.e., the larger the misfit the narrower the strips A and B.

Perfect periodic fit will be achieved in lamella (I), with sequence nA, nB, if the relation,

$$n(d_p - d_A) + m(d_p - d_B) = 0, \quad [3]$$

is satisfied as well as the relations [1] and [2]. The period Λ is then exactly

$$\Lambda = (m + n)d_p. \quad [4]$$

However, for symmetry reasons a condition similar to (3) applies to lamella (II). The condition for perfect periodic fit is now

$$m(d_p - d_A) + n(d_p - d_B) = 0. \quad [5]$$

The set of homogeneous Eqs. [3] and [5] has a nontrivial solution for m and n only if the determinant of the coefficients is zero. This will be the case if

$$d_p = 1/2(d_A + d_B). \quad [6]$$

The solution of the set [3] and [5] for this value of d_p is then

$$m = n = \Lambda/2d_p \quad [7]$$

(i.e., as concluded above on intuitive grounds, only the symmetrical situation represented in Fig. 5b is consistent with perfect periodic strain compensation and moreover relations [1] and [2] must be satisfied).

However, in general this solution [7] will not be an integral number, i.e., Λ may be incommensurate with d_p. The next best integral approximation may then be that m and n differ by one unit such that

$$n < \frac{\Lambda}{2d_p} < n + 1$$

$$m < \frac{\Lambda}{2d_p} < m + 1. \quad [8]$$

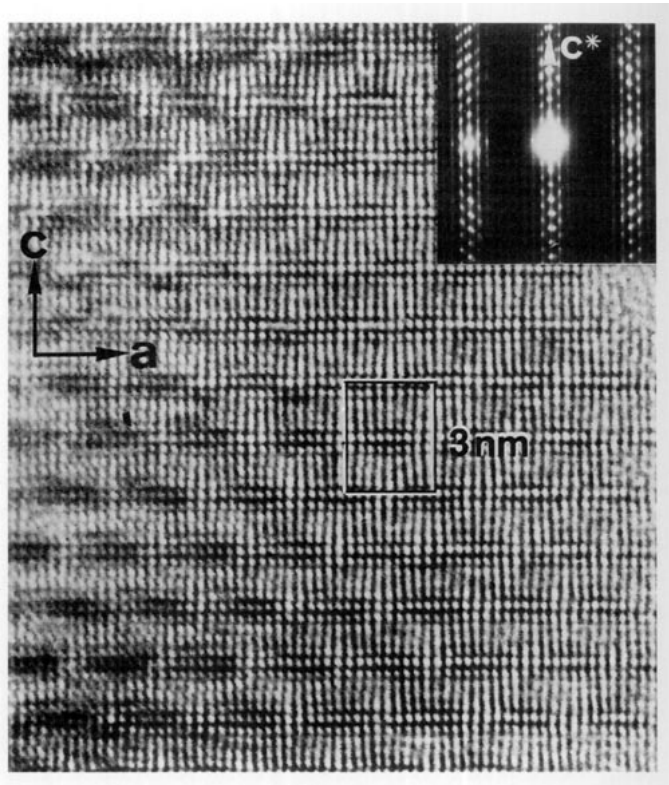

FIG. 9. HREM image of the 2212-BSCCO compound, showing a clear spacing modulation.

These essentially geometrical considerations suggest that the structure with equal width of the strips if preferred but they also allow for more complicated sequences in which the strip widths differ by one unit, as observed experimentally in Figs. 2 and 3. If $d_P - d_B < d_A - d_P$ the limiting strain ε_m in strips of the type B will only be reached for a larger width than for type A strips. Strips of inequal width tend to form, at the expense of nonstoichiometry consisting in an excess of B (Fig. 5d). This nonstoichiometry limits the difference in widths of A and B strips.

If the mismatch between adjacent lamellae is too large and (or) the lamellae are not sufficiently compressible to be accommodated elastically, "interfacial" or "misfit" dislocations will be formed. this case will be addressed in a forthcoming paper.

High resolution images of $Bi_2Sr_2CaCu_2O_8$ such as the one shown in Fig. 9 demonstrate that the $(BiO)_2$ lamellae consist of alternating strips, parallel to [100], exhibiting two different interdot spacings (see e.g. (8, 9)). The alternation of the strips is in antiphase in successive layers. The dot spacing at the level of the CuO_2 plane has an intermediate value, between the two extreme spacings within the alternating strips in the $(BiO)_2$ lamellae. The conditions for the applicability of the model described above are thus realized. Unfortunately these observations do not allow us to conclude unambiguously as to the origin of the variation

of spacings in the $(BiO)_2$ lamellae. It has previously been proposed that the spacing differences may result from differences in oxygen contents; regions of excess oxygen in interstitial positions give rise to local dilatation of the lattice. The excess oxygen in turn was assumed to be caused by the fact that the equilibrium bond length BiO is too small to fit perfectly on to the perovskite block. The BiO layers are thus under tensile stress. These stresses can be relieved by the incorporation of interstitial oxygen. Excess oxygen has in fact been detected (10) in modulated samples of $Bi_2Sr_2CaCu_2O_{8+\delta}$.

In an alternative model the variation in $d(010)$ spacing is attributed to differences in orientation of the lone (inert) electron pairs associated with the Bi^{3+} ions. The spacing would be largest when the lone pair electron cloud is oriented along the [010] direction. This would simultaneously cause the c spacing of the layers to be small. In the opposite case, where the lone pairs are oriented in a direction perpendicular to the layers, the (010) spacing would be smallest and the c separation of the layers largest. The two models can be reconciled by assuming that the lone pairs are preferentially directed with respect to excess oxygen atoms, leading to the same periodic variation. Whatever be the origin of the spacing differences along the b direction the present model suggests that the wavy shape of the layers results from the strain energy minimization principle.

APPLICATION OF THE MODEL

Due to the lack of systematic measurements of the effect of the composition of the (Hg, Pb, Tl)O_δ and (Ba, Sr)O layers on the modulation direction and modulation period, it is at present not possible to offer a detailed quantitative comparison with the model. A major difficulty is that it is often not possible to find an experimental value for the unrelaxed interplanar distances d_A, d_B, and d_P because no adequate crystal structure exists. Moreover the layers often contain several different cations. One has then to rely on Vegard's law to estimate the lattice parameter. However, Vegard's law may often be seriously in error. It is nevertheless possible to verify whether or not the trends predicted by the model are borne out in actual fact by the observations. In two such cases a comparison is possible.

From the image of Fig. 3 the configuration of the ion rows in the HgO_δ layers can be easily deduced. As mentioned above, the prominently bright dots which are known from simulated images to represent CO rows are visibly more widely spaced than the weakly bright dots in the strips which are assumed to image the (HgTl)O columns. This conclusion remains valid even if the atom columns would in fact be imaged as dark dots. The outer dots of the linear clusters of four prominent bright dots are often somewhat less bright, suggesting partial substitution of C–O by (Hg, Tl)O in the corresponding columns. Connecting the weakly bright dots with the prominently bright dots in the way represented in Fig. 4 visualizes the strain to which the perovskite lamella is subjected. These observations strongly suggest that the 100 spacing in the CO strips is larger than that in the (HgTl)O layers. The situation (i), i.e., $d_A < d_P < d_B$, is thus realized (A = (Hg, Tl)O; B = CO). The perovskite lattice planes parallel to (001) are thus deformed as shown in Fig. 4 and the layers which are roughly normal to the planes thus become slightly wavy.

The modulation in the two compounds,

$$(Hg_{0.3}Tl_{0.7})(Sr_{1.5}Ba_{2.5})Cu_2CO_3O_{7-\delta}\,(I)$$

$$(Hg_{0.3}Tl_{0.7})(Sr_{2.5}Ba_{1.5})Cu_2CO_3O_{7-\delta}\,(II),$$

is along $[100]_P$ and the wavelengths are, respectively, $\lambda \approx 6.50$ in (I) and $\lambda \approx 7.0$ in (II). The composition of the HgO_δ layer is kept constant whereas the composition of the perovskite layer is different. Replacing barium by strontium, which has a smaller ionic radius than Ba, leads to a somewhat smaller interplanar spacing d_{100} of the perovskite lamellae. Since the Hg^{2+} and Tl^{3+} ions are substantially smaller than Ba^{2+} and Sr^{2+}, we must assume that the (Hg, Tl)O layers are under tensile stress. The substitution of the barium by the strontium thus decreases the residual tensile strain and thus should lengthen the modulation period, as observed.

Qualitative verification of the model is also possible in the series of compounds $Bi_2Sr_{2-x}La_xCaCu_2O_{8+\delta}$ for which data are available in the literature (11). The modulation wavelength is found to vary from $\lambda = 4, 7b$ for $x = 0$ to $=3, 4b$ for $x = 1, 2$. Substitution now affects the perovskite lamellae; Sr $\rightarrow$ La substitution leads to an increase in the b parameter which is essentially determined by the perovskite lamellae (11). Since the BiO layer in the $x = 0$ compound is under tensile stress with respect to the juxtaposed perovskite lamellae, an increase in d_P increases the difference in interplanar spacing $d_P - d_B$ and hence shortens the modulation period, as observed.

REFERENCES

1. F. Goutenoire, M. Caldes, A. Maignan, C. Michel, M. Hervieu, and B. Raveau, *Physica C* **208,** 121 (1993).
2. Y. Matsui, M. Ogawa, M. Uehara, H. Nakata, and J. Akimitsu, *Physica C* **217,** 287 (1993).
3. M. Kikuchi, E. Ohshima, N. Ohnishi, Y. Muroaka, S. Nakajima, E. Aoyaga, M. Ogawa, J. Akimitsu, T. Oku, K. Hiraga, and Y. Syono, *Physica C* **219,** 200 (1994).
4. M. Uehara, S. Sahoda, H. Nakata, J. Akimitsu, and Y. Matsui, *Physica C* **222,** 27 (1994).
5. M. Huvé, G. Van Tendeloo, M. Hervieu, A. Maignan, and B. Raveau, *Physica C* **231,** 15 (1994).
6. M. Hervieu, C. Michel, M. Huvé, C. Martin, A. Maignan, and B.

Raveau, *Microsc. Microanal. Microstruct.* **4** 41 (1993).
7. G. Van Tendeloo and S. Amelinckx, *Phys. Status. Solidi A* **43,** 553 (1977).
8. G. Van Tendeloo, H. W. Zandbergen, J. Van Landuyt, and S. Amelinckx, *Appl. Phys. A* **46,** 153 (1988).
9. O. Eibl, *Physica C* **168,** 215 (1990).
10. A. Q. Pham, M. Hervieu, A. Maignan, C. Michel, J. Provost, and B. Raveau, *Physica C* **194,** 243 (1992).
11. H. W. Zandbergen, W. A. Groen, G. Van Tendeloo, and S. Amelinckx, *Appl. Phys. A.* **48,** 305 (1989).